Structural transitions at high pressure and metastable phase in Si0.8Ge0.2

M. Gerin, D. Machon, S. Radescu, Sylvie Le Floch, Y. Le Godec, T. Gaudisson, F. Alabarse, P. Veber, R. Debord, D. Amans, et al.

▶ **To cite this version:**

M. Gerin, D. Machon, S. Radescu, Sylvie Le Floch, Y. Le Godec, et al.. Structural transitions at high pressure and metastable phase in Si0.8Ge0.2. Journal of Alloys and Compounds, 2023, 954, pp.170180. 10.1016/j.jallcom.2023.170180 . hal-04079665

HAL Id: hal-04079665
https://hal.science/hal-04079665

Submitted on 3 Nov 2023

HAL is a multi-disciplinary open access archive for the deposit and dissemination of scientific research documents, whether they are published or not. The documents may come from teaching and research institutions in France or abroad, or from public or private research centers.

L'archive ouverte pluridisciplinaire **HAL**, est destinée au dépôt et à la diffusion de documents scientifiques de niveau recherche, publiés ou non, émanant des établissements d'enseignement et de recherche français ou étrangers, des laboratoires publics ou privés.

Structural transitions at high pressure and metastable phase in $Si_{0.8}Ge_{0.2}$

M. Gerin[1], D. Machon[1,2,3]*, S. Radescu[4], S. Le Floch[1], Y. Le Godec[5], T. Gaudisson[1], F. Alabarse[6], P. Veber[1], R. Debord[1], D. Amans[1], V. Pischedda[1]*

[1] *Institut Lumière Matière, UMR5306 Université Lyon 1-CNRS, Université de Lyon 69622 Villeurbanne cedex, France*

[2] *Laboratoire Nanotechnologies et Nanosystemes (LN2), CNRS UMI-3463, Université de Sherbrooke, Institut Interdisciplinaire d'Innovation Technologique (3IT), Sherbrooke QC J1K 0A5, Quebec, Canada*

[3] *Institut Interdisciplinaire d'Innovation Technologique (3IT), Université de Sherbrooke, 3000 Boulevard Université, Sherbrooke, J1K OA5, Québec, Canada*

[4] *Departamento de Física and Instituto de Materiales y Nanotecnología, MALTA Consolider Team, Universidad de La Laguna, E38200 San Cristóbal de La Laguna, Tenerife, Spain*

[5] *Institut de Minéralogie, de Physique des Matériaux et de Cosmochimie (IMPMC), Sorbonne Université, UMR CNRS 7590, Muséum National d'Histoire Naturelle, IRD UMR 206, 75005 Paris, France.*

[6] *Elettra - Sincrotrone Trieste S.C.p.A., 34149 Basovizza, Trieste, Italy*

Corresponding authors: denis.machon@univ-lyon1.fr, vittoria.pischedda@univ-lyon1.fr

Abstract

The high-pressure behaviour of $Si_{0.8}Ge_{0.2}$ alloy is explored using *in situ* Raman spectroscopy, X-ray diffraction techniques and density functional theory (DFT) simulations. High pressure experiments revealed a pressure-induced transition from the stable cubic semiconducting phase (dc- $Si_{0.8}Ge_{0.2}$) to the tetragonal β-tin metallic phase (β-$Si_{0.8}Ge_{0.2}$) during compression. This sluggish transition is significantly accelerated at moderate temperature (<300°C). Upon decompression, successive transitions towards metastable phases are observed. A first transition from the metallic β-$Si_{0.8}Ge_{0.2}$ toward the rhombohedral r8-$Si_{0.8}Ge_{0.2}$ phase is observed at 10.3 GPa followed by a partial transition to the body-centered cubic bc8-$Si_{0.8}Ge_{0.2}$ phase at 2.2 GPa. After releasing the pressure, r8 and bc8 phases coexist at ambient conditions. This transition pathway is similar to that followed by pure silicon and is consistent with the *ab initio* enthalpy calculations. This phase transition sequence is confirmed by *in situ* Raman spectroscopy, where signatures of r8 and bc8 phases are observed in the Raman spectra at decompression. An *ab initio* simulation method is proposed to assign the Raman spectrum of $Si_{0.8}Ge_{0.2}$ alloy using group theory and projection operators. The exploration of metastable states in these alloys is of major interest both in terms of applications (e.g. optoelectronics) and from a

fundamental point of view to better understand the effects of alloying on the physical properties (e.g. vibrational).

I. Introduction

Applying extreme conditions on materials can lead to metastable structures with attractive physical properties. Group IV elements, such as carbon, silicon and germanium are known to exhibit polymorphism under pressure, and they can exist in different metastable phases after pressure cycling. The carbon diamond phase is the typical example of a metastable phase at ambient conditions, obtained by pressure-temperature treatment, and which has drastically different physical and chemical properties compared to the stable graphite phase. Silicon and germanium exhibit a rich pressure-temperature phase diagram. One of their peculiarities is the decrease of the melting temperature with increasing pressure, a situation that goes against the usual tendency found using the Clapeyron equation for melting. Another interesting aspect of the pressure-induced phase transitions in Si and Ge is the rich polymorphism of metastable phases.

Silicon and germanium are known to transform from the semiconducting diamond structure to the metallic β-tin phase in the range of 8-10 GPa [1]–[6]. New metastable phases were observed during the decompression from this metallic phase [7]–[11]. Depending on the conditions of decompression, transition pathways in germanium and silicon differ. On the one hand, germanium transforms to a tetragonal structure (st12-Ge) at around 8 GPa under non-hydrostatic conditions and slow unloading [1], [8], [12], [13]. In case of fast hydrostatic unloading, germanium tends to form a distorted body-centered rhombohedral structure (r8-Ge) at ~7 GPa followed by a transformation to a body-centered-cubic structure (bc8-Ge) at ~0.5 GPa [7], [8]. Then, bc8-Ge rapidly transforms at ambient pressure to a hexagonal diamond phase [2], [14], [15]. Silicon, on the other hand, is known to transform into the r8-Si phase at ~10 GPa, and then to the bc8-Si phase (~3 GPa) upon decompression, regardless of hydrostaticity [10], [11]. Contrary to germanium, r8-Si and bc8-Si phases are relatively stable at ambient conditions and only transform into hexagonal silicon at temperatures of ~200°C [2].

Si_xGe_{1-x} alloys are an example of solid solutions with perfect miscibility. In their stable cubic diamond structures, they have interesting properties. Tunability of physical properties such as the bandgap [16] or thermal properties [17] make them materials of choice for a wide range of applications. They are used for energy conversion in the space industry due to their thermo-electric properties [18]–[20], in solar cells [21], in photonic [22] or microelectronics [23]. They also show synergistic effects when used as anode active material in Li-ion batteries [24] combining the very high storage capacity of lithium in silicon with the high electronic and Li ion conductivity in germanium [25] . More recently, an hexagonal structure showing a tunable direct bandgap has received a huge interest because of potential applications in optoelectronics [26]. The hexagonal phase is obtained by heteroepitaxial growth of Si_xGe_{1-x} on a nanowire of GaAs [26] and, interestingly, can be

also synthesized by high-pressure and high-temperature (HP-HT) treatments [2], [27]–[29].

Surprisingly, while the amount of work dealing with phase transitions and transformations in pure silicon and germanium during the pressure cycle is significant, there are far fewer experimental studies on the high pressure (HP) behaviour of Si_xGe_{1-x} alloys, and on the formation of their metastable phases after a pressure cycle. Pressure-induced phase transition to the metallic β structure has been reported in Si_xGe_{1-x} both theoretically [30], [31] and experimentally [32]. A primitive hexagonal phase was also observed at higher pressure (> 14 GPa) and the transition pressure depends on the Ge content in the alloy [33]. Upon decompression, metastable phases in Si_xGe_{1-x} have been observed for Ge dominant alloys (up to x= 0.13) and Si-doped Ge alloys (up to x= 0.974) [34]. According to this study, the behaviour of the alloys follows that of the main component (Ge in case of Ge dominant alloy and Si in case of Si dominant alloy). The possibility to recover metastable phases was also observed by ex-situ HP-HT experiments for different SiGe compositions [29].

Furthermore, a challenging aspect in the study of Si_xGe_{1-x} alloys is the correct description of their Raman spectra. Indeed, in the solid solution, some local substitutional disorder is introduced into the structure, although the overall symmetry remains cubic. Here, we propose the Raman spectrum of Si_xGe_{1-x} alloys can be interpreted using a description of the band unfolding method based on the projection operators as shown by Ikeda *et al.* [35], [36]. The assignment of the Raman modes can be obtained by projecting the phonon frequencies of the disordered alloy (without symmetry) into the irreducible representations of the given “ordered” structure.

In this work, pressure-induced phase transitions in $Si_{0.8}Ge_{0.2}$ are investigated. The goals of this study are manifold :1) to determine the elastic and vibrational properties of the low-pressure, diamond structure, phase; 2) to identify the (metastable) phases formed during pressure cycle; and 3) to assign the Raman spectra of the different phases using *ab initio* simulations that account for the local and global organization using the method of projection operators.

The article is organized as follows. After describing the methods in section II (synthesis, high-pressure techniques and *ab initio* simulations), *in situ* X-ray diffraction (XRD) and Raman spectroscopy experiments are reported in section III. First, the ones performed using a Paris-Edinburgh (PE) press on a synchrotron light source, including the effect of annealing at high pressure (Section III.A), second, the HP experiments in a diamond-anvil cell (DAC) using an X-ray lab source (Section III.B). The last section (Section III.C) is dedicated to the results obtained by *in situ* Raman spectroscopy during pressure cycles in DAC. The experimental results are complemented with *ab initio* simulations to assign the different modes observed in the Raman spectra.

II. Methods

Materials

200 mg of silicon powder from Strem chemicals (purity: 99.999%) and germanium powder from Sigma Aldrich (purity: 99.999%) was mixed in the atomic ratio 80:20 using an agate mortar and a crucible under protective atmosphere (step 1). The resulting mixture was pressed to form pellets 2 mm high and 8 mm in diameter (step 2). They were placed inside an alumina crucible which was then inserted inside an alumina tube of a horizontal Carbolite (STF 16/180) oven. Zirconium was also inserted as a local reductant due to its strong affinity with oxygen (step 3). To further protect the sample from oxidation, the tube atmosphere was pumped and filled with argon several times before annealing, and a continuous flow of argon was used during the experiment. Between each one-hour annealing at different temperatures, grinding and compaction (steps 1 and 2) were repeated. Starting from 1000°C, the temperature was successively increased to 1100°C, 1200°C, 1250°C, and finally to 1350°C. Energy Dispersive X-Ray analysis (EDX) on the sample gives a Si:Ge ratio of 0.79(2):0.21(2) (see Fig. S1) in agreement with Raman spectroscopy analysis (see Section III. C). No sign of oxidation or any contamination were detected on the synthesized samples by EDX analyses. Ambient diffraction pattern of the $Si_{0.8}Ge_{0.2}$ is shown in Figure 1. Patterns can be indexed by Le Bail refinement using the diamond-type structure with a cell parameter *a* = 5.458(1) Å in perfect agreement with the literature (PDF file n°04-022-2155 for $Si_{0.8}Ge_{0.2}$). The measured cell parameter is also in agreement with the Vegard's law considering the composition $Si_{0.8}Ge_{0.2}$ [39].

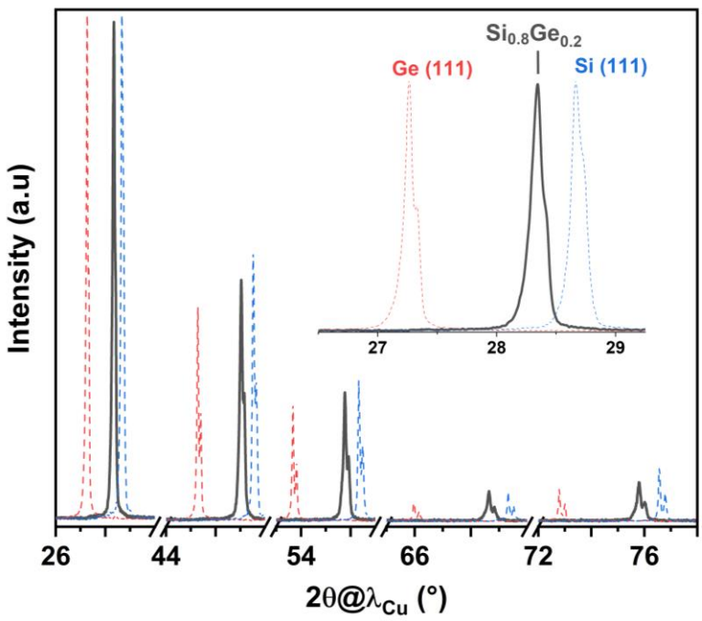

Figure 1 – XRD pattern of $Si_{0.8}Ge_{0.2}$ at ambient conditions to be compared with simulated Ge and Si patterns. Shoulders in the diffraction peaks are due to the splitting of Cu $K\alpha_1$ and $K\alpha_2$ radiation. Cell parameter obtained using Le Bail refinement is *a* = 5.458(1) Å.

High pressure characterization methods

In situ synchrotron XRD measurements under HP conditions were performed using a PE press at the Xpress beamline of the Elettra Synchrotron Facility (Trieste, Italy). The

pressure/heating device is composed of the PE press, a hydraulic pump and a low voltage - high current power supply. Using opposed conical sintered diamond anvils, this system can achieve pressure up to 16 GPa and temperature over 1000°C [40]. The $Si_{0.8}Ge_{0.2}$ sample was placed inside a boron-nitride capsule of 0.8 mm inner diameter and 2 mm high, surrounded by a graphite furnace. This assembly was then inserted into an X-ray transparent gasket (boron-epoxy composite), which serves as a thermal and electrical insulator as well as the pressure transmitting medium (PTM). The boron-epoxy composite gasket offers quite good hydrostatic conditions for this type of sample configuration. From in situ X-ray diffraction measurements on powdered NaCl loaded into a boron-epoxy gasket, Gauthier et al. estimated that the average deviatoric contributions were less than 5% below 10 GPa [41].

XRD patterns were obtained using an 80 µm focused monochromatic X-ray beam of λ= 0.4958 Å. Good quality 2D diffraction patterns were collected in 80 s on a PILATUS3 S6M detector (from Dectris). The pressure calibration curve at room temperature was checked by using silicon powder in the same environment (Fig. S2), upon compression up to an oil pressure of 600 bars and using the silicon Equation Of State (EOS) [6].

Complementary *in situ* XRD HP experiments using a lab source were performed using a flat Almax-type DAC with 600 µm diameter diamond culets. The sample was placed inside a 250 µm chamber drilled in an indented stainless-steel gasket (thickness = 80 µm), along with a ruby acting as a pressure gauge. The pressure was calculated using the known dependence of the ruby luminescence line with pressure [42]. Paraffin oil was used as PTM. The DAC has an aperture angle of 85° (top and bottom). We used a molybdenum source (λ= 0.70926 Å) and a beam of approximately 150 µm in diameter, in a microfocus Oxford Xcalibur Mova diffractometer.

Because the sample was slightly textured and the experimental setup in the lab did not allow the cell to be rotated during data acquisition in order to average crystallite orientations and obtain a better statistic, the quality of the XRD pattern was not sufficient for robust Rietveld refinement and Le Bail refinements on the 1D integrated diffraction patterns were done to extract cell parameters.

Raman spectra were recorded using a homemade spectrometer in backscattering geometry. The laser wavelength used was 532 nm, the laser power was initially adjusted to 2 mW at the entrance of the objective in order to avoid heating effects on the sample and to improve signal over noise ratio. The laser beam was focused with a 50x objective and the signal was dispersed by a grating of 1800 grooves/mm. The signal was collected on a Princeton Instruments Acton SP-2500i spectrometer. The spectral resolution of the setup is estimated to ~1 cm^{-1}.

In situ Raman spectroscopy measurements under high pressure conditions were conducted using a Letoullec-type DAC with 600 µm diameter diamond culets [43]. The sample chamber and sample environment were prepared in the same way as for the XRD experiment using a flat Almax DAC. Paraffin oil, used as PTM, is quasi-hydrostatic up to 3-4 GPa [44] and its Raman activity does not interfere with the main Raman modes of the sample. The HP Raman experiment was performed when the loaded samples showed homogeneity to avoid discrepancies due to variation in positions due to composition.

Simulations

Si_xGe_{1-x} can be considered as a random alloy whose lattice parameters depend on the composition according to the Vegard's law [45]–[47]. The Raman spectra of Si_xGe_{1-x} alloys can be simulated within the harmonic approximation using a cluster expansion method [48], [49]. Due to the disorder associated with the solid solution, the symmetry of the simulation clusters is normally different (usually lower) than that of the crystallographic phase. Within the cluster expansion method, the supercells used for the phonon calculation of a disordered alloy normally lack the (average) crystallographic symmetry of the real alloy. This makes difficult to assign the calculated vibrational modes and to compare them with those from experiments. As an example, a typical simulation supercell has only the trivial identity as a symmetry operation and is then described by the space group P1. In this case, all the calculated modes at the centre of the Brillouin zone of the simulated alloy would be both Raman and infrared active, a situation that does not correspond to the experimental observations. A possible solution is to use the projection operator method which consists in decomposing the modes of the disordered structures according to the irreducible representation of the modes of the underlying "ideal-ordered" structure [35], [36]. With this scheme, the modes obtained at the Brillouin zone centre can be analysed in a form quite similar to that of an ordered system (with its crystallographic symmetry). The positions of the peaks in the spectral function curve obtained by the unfolding method, which reflect the crystallographic symmetry, are related to the frequencies of the studied disordered structure.

Based on our previous work [12], all the Density Functional Theory (DFT) simulations for the analysis of the $Si_{0.8}Ge_{0.2}$ alloy were performed using the Vienna *ab initio* simulation package (VASP) [50]–[53].We used a projector-augmented-wave scheme (PAW) and explicitly included the semi-core *d*-electrons of Ge as well as the outermost *s* and *p*-electrons, adopting the so-called PBEsol generalized gradient approximation (GGA) for the exchange and correlation functional [50]. The cut-off in the plane wave basis set was taken at 375 eV. For the integration over the Brillouin zone, we used a 10x10x10 Monkhorst-Pack grid. The $Si_{0.8}Ge_{0.2}$ alloy was simulated using the ATAT cluster expansion scheme [48], [49] with cluster sizes up to 16 atoms, which is necessary to obtain accurate cluster convergence (the cross validation score was 0.34 meV).

In order to identify the vibrational modes of the Si_xGe_{1-x} alloy (with an experimental value of x of about 0.8), appropriate supercells according to each symmetry were employed. 16-atom supercells were used for bc8 and r8 structures (corresponding to the stoichiometric composition $Si_{0.8125}Ge_{0.1875}$) whereas 8-atom supercells were used for the diamond and β phases (corresponding to $Si_{0.75}Ge_{0.25}$). These simulated compositions are closed enough to the experimental ones to allow comparison between theory and experiments. To calculate the phonon frequencies, we used a post processing Phonopy package to analyze the vibrational modes and the structure plots were done with VESTA [54], [55].

III. Results & discussion

A. *In situ* HP-HT synchrotron XRD study using a PE press

$Si_{0.8}Ge_{0.2}$ was first studied at HP and high temperature (HT) using a PE press at the Xpress beamline (Elettra Synchrotron Facility). Evolution of $Si_{0.8}Ge_{0.2}$ diffraction patterns with pressure are shown in Figure 2. During compression, the diffractograms can be indexed with the diamond structure (named hereafter dc-$Si_{0.8}Ge_{0.2}$) up to ~7.4 GPa. Additional features due to graphite and h-BN can also be observed and identified. Above this pressure, a phase transition is observed with the appearance of a weak signal at $2\theta \sim 12°$. Interestingly, this transition is concomitant with the strong reduction of the full width at half maximum (FWHM) of the diamond phase diffraction peaks (Figure 2.b). This effect is due to an elastic relaxation associated with a phase transition and has already been observed in germanium during the semiconductor-to-metal transition [4], [12]. Such behaviour was also observed for pure silicon during the calibration of the PE press (Figure S2). The metallic character of the high-pressure phase was confirmed by electrical resistance measurements (Figure 2.c), performed in a separate experiment, using two electrodes placed at the top and bottom of the anvils of the PE press. A drop in the resistance of more than four orders of magnitude is observed across the transition. This result is similar to what was observed in silicon or germanium [10], [56].

With increasing pressure, the signal from the HP phase increases and can be assigned to the tetragonal structure β-tin (β-$Si_{0.8}Ge_{0.2}$). This phase transition is similar to that observed for silicon and germanium. The onset transition pressure at ~7.4 GPa appears to be in agreement with reported theoretical values for Si (~7.5 GPa) [57]–[59] but below the theoretical values obtained by Soma & al. (~12±2 GPa) [30] and the experimental values reported by Werner & al. (~12 GPa) [60] for solid solutions. The beginning of the transition at rather low pressure can be attributed to: i) the presence of shear stresses induced on the sample by the non-hydrostatic conditions, that are known to lower the transition pressure [4]; ii) a different way to define the transition pressure. By indirectly measuring the relaxation in the sample, we were able to detect the transition earlier and more accurately. Indeed, this relaxation is believed to occur at a very early stage of the transition when the β-phase begins to nucleate. In ref. [60], the onset of the transition is defined by the equality between the intensity of the dc-Si_xGe_{1-x} (111) peak and that of β-Si_xGe_{1-x} (200) peak for different compositions. By taking this definition, the diamond-to-β phase transition occurs at 12 GPa in our case, in very good agreement with previous works.

During this compression step, β-$Si_{0.8}Ge_{0.2}$ mass ratio increases from 20% at 12.3 GPa to 36% at the maximum reachable pressure of 14.2 GPa, where diamond- and β-$Si_{0.8}Ge_{0.2}$ phases still coexist. This large domain of coexistence is attributed to the sluggish character of the transition related to the strong first order character of the transition [61], [62].

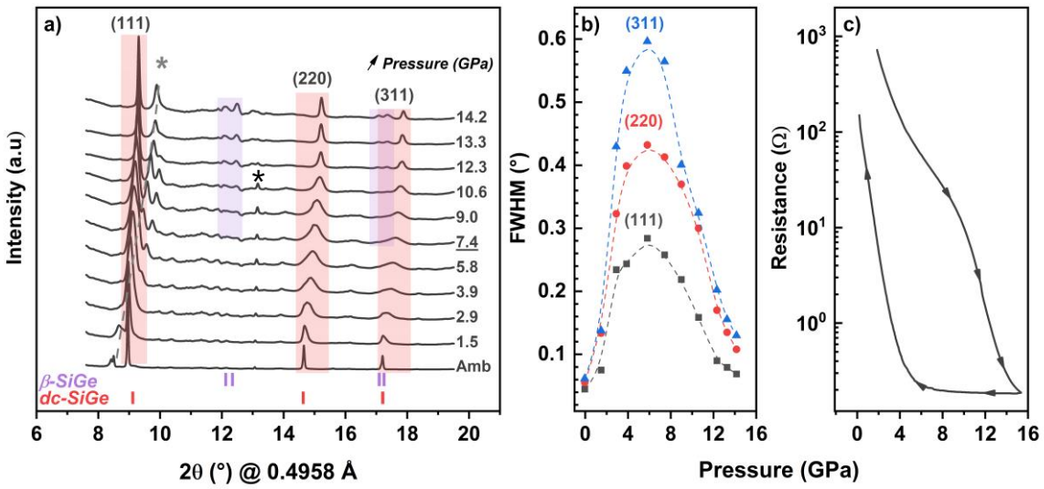

Figure 2 - a) XRD patterns of $Si_{0.8}Ge_{0.2}$ upon compression in a PE press. The peaks under the asterisk represent the contribution of the gasket (h-BN and graphite). b) Evolution of FWHM of the three most intense reflections of $Si_{0.8}Ge_{0.2}$ with pressure, showing a maximum relaxation at ~7.4 GPa when the phase transition starts. c) Electrical resistance measurements during compression and decompression cycling in PE press.

β-$Si_{0.8}Ge_{0.2}$- unit cell parameters at 12.3 GPa are *a* = 4.68(1) Å and *c* = 2.59(1) Å, with *c/a* = 0.55(1) in agreement with ref. [30]. This is consistent with a linear interpolation of the *a* and *c* parameters of β-Si and β-Ge obtained from our simulation data (Tab. S1).

A plot of V/V_0 as a function of pressure is shown in Figure 3. These data were initially fitted using a second-order Birch-Murnaghan (BM2) equation of state model and led to K = 92(1) GPa. In a second step, a third-order Birch-Murnaghan (BM3) equation of state model was used with K' fixed to 4.24. This K' value was chosen so that the resulting bulk modulus could be compared with the recent data obtained on Si by Anzellini *et al.* [6]. We obtained K = 91(1) GPa, which is in very good agreement with the expected value based on a linear interpolation between bulk modulus and composition (Table I).

Using DFT simulations, the calculated bulk modulus (and its first derivative) for the diamond phase is 93.9 GPa (K'=4.0), 69.6 GPa (K'=4.1) and 88.6 GPa (K' =3.9) for Si, Ge, and $Si_{0.75}Ge_{0.25}$, respectively, values that are in excellent agreement with the experimental ones.

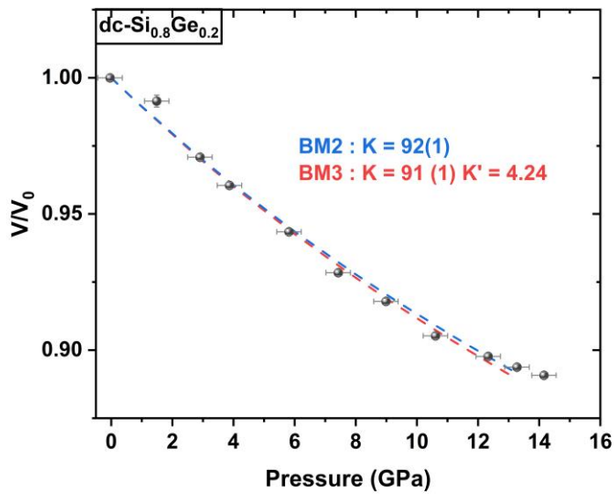

Figure 3 - V/V_0 plot for $Si_{0.8}Ge_{0.2}$ as a function of pressure (points) along with a second-order with K' parameter fixed at 4 (blue dotted line) and a third-order Birch-Murnaghan EOS fitted to the data (red dotted line).

Table I - Comparison of reported bulk modulus for the diamond structure of Si, Ge and $Si_{0.8}Ge_{0.2}$

Sample	K (GPa)	K'	PTM	Method	Ref.
Si	101.5	3.45	He	XRD, DAC	[6]
Si	96.86	4.24 (fixed)	He	XRD, DAC	[6]
Si	99.90	3.80	4:1 eth:meth	XRD, DAC	[63]
Si	97.88	4.23		Ultrasonic	[64]
Si	96	3.9	1:1 ethyl:methyl	XRD, cubic anvil press	[65]
Ge	74.37	4.76		Ultrasonic	[64]
Ge	76.0	4.373	4:1 eth:meth	XRD, DAC	[1]
Ge	74.9	3.0	4:1 eth:meth	XRD, DAC	[1]
$Si_{0.8}Ge_{0.2}$	93.7			Ultrasonic	[66]
$Si_{0.8}Ge_{0.2}$	92(1)	4.00 (fixed)	Boron-epoxy	XRD, PE	This work
$Si_{0.8}Ge_{0.2}$	91(1)	4.24 (fixed)	Boron-epoxy	XRD, PE	This work

As the transition is still incomplete at 14.2 GPa, and dwelling time does not affect the phase proportion, temperature was augmented from 25°C to 255°C in 30 min with 10 min steps at 170°C and 200°C. During these heating steps, pressure was maintained constant at 14.2 GPa. Diffraction patterns in Figure 4 show that heating results in a rapid increase of the β-$Si_{0.8}Ge_{0.2}$ phase proportion, indicating that the energy barrier between the two phases is very low at this pressure.

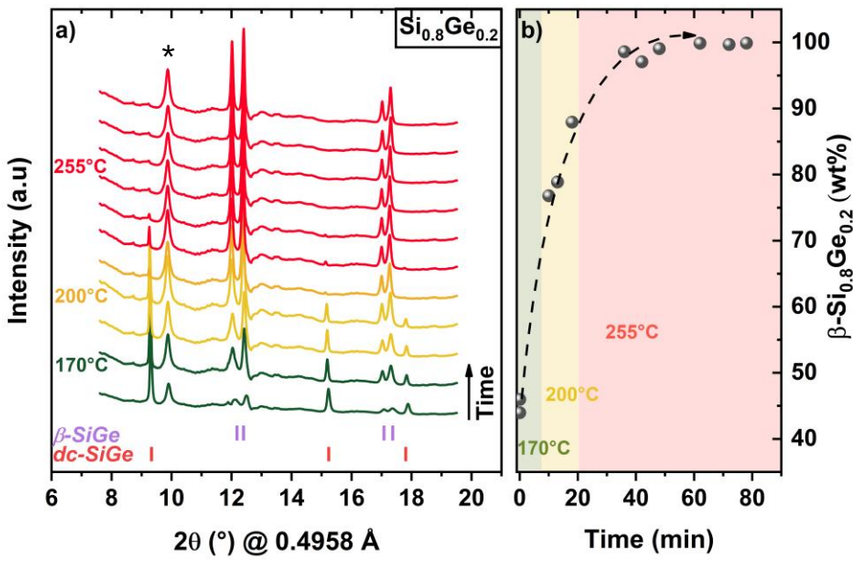

Figure 4 - a) XRD patterns of $Si_{0.8}Ge_{0.2}$ obtained upon isobaric heating from 25 to 255 °C at 14.2 GPa. The peak under the asterisk represent the contribution of the gasket. b) Weight fraction of β-$Si_{0.8}Ge_{0.2}$ as function of annealing temperature and time.

After 1 hour at 255°C, no reflection from the diamond phase can be measured anymore, indicating the full transformation of the diamond phase to the β phase. This metallic phase appears to be stable after decreasing the temperature and staying one night at ambient temperature and 14.2 GPa. It is worth noting that no chemical decomposition was observed under HP and HT. It has been observed that pressure may lead to a ΔV in alloys energetically favouring the chemical decomposition and the emergence of components (end-members of the solid solution) [67].

We decompressed $Si_{0.8}Ge_{0.2}$ from 14.2 GPa at constant temperature (255°C) with the intention of improving the kinetics of the phase transformations to potentially new metastable phases. However, only a reverse β-to-diamond transition was observed at ~10.0 GPa. The two phases coexist down to ~5.7 GPa (Figure S3). From this pressure to ambient conditions, only the diamond phase is observed. No appearance of metastable phases was observed in this experiment. This is certainly due to the effect of temperature that ensures a thermodynamic pathway and prevents the formation of metastable phases. It is well documented that in silicon, germanium and alloys, under certain conditions, different metastable phases can be observed [68], [69]. They are usually formed with the help of shear stresses associated to non-hydrostatic conditions [8], [10], conditions we considered with the other XRD experiments we performed using a DAC and cold pressure cycles.

B. *In situ* XRD at HP using a DAC

A second experiment using a DAC with paraffin oil used as the PTM (providing hydrostatic conditions up to ~4 GPa [44]) was conducted. The compression up to 17.2 GPa (Figure S4) of the diamond-$Si_{0.8}Ge_{0.2}$ phase was covered rapidly, the focus being on characterizing the metallic β-phase and the transition sequence on subsequent decompression. During compression, the phase transition from diamond to the β-phase is

observed above ~10.0 GPa. Coexistence between the two phases extends from 10 GPa (~1 wt% of β-$Si_{0.8}Ge_{0.2}$) to 17.2 GPa (fully transformed). The wide pressure range of phase coexistence is similar to that of silicon [6], [9], [63], [70] and germanium [1], [4]. No new phase transitions were observed up to 17.2 GPa, the highest pressure reached in this experiment and no evidence of additional phases such as orthorhombic or hexagonal was detected in our case, although they were observed for Si in this pressure range [33], [69], [71].

XRD patterns in DAC during decompression are shown in Figure 5a. A first transition is observed at ~10.3 GPa with clear new reflections appearing at 2θ~15° and 2θ~9°. This pattern can be successfully indexed with a r8 structure, as in the case of silicon where this structure was observed at a similar pressure [11], [72]**.** The measured cell parameters are *a* = 9.16(1) Å and *c*= 5.41(1) Å, in agreement with the values obtained by DFT calculations (*a* = 9.17 Å and *c* = 5.43 Å) of the r8-phase. Phase proportions indicate that β and r8 phases coexist between 10.3 and 5.4 GPa (Fig.5b). In pure silicon, a full transition to r8 phase was reported at around 6.2 GPa [11] and 8.2 GPa [72] under more hydrostatic conditions.

At lower pressure, the rhombohedral r8 phase partially transforms to another phase that can be indexed as the body-centered cubic structure (bc8). Pure bc8 was recovered for elemental Si and Ge [7], [9], [73], [74] and $Si_{0.8}Ge_{0.2}$ and binary [29], [75].

Diffraction peaks of bc8 and r8 phases are close to each other. However, the reflection at 2θ~9° is only explained by the presence of the r8 phase at ambient pressure i.e., in our case, bc8 and r8 coexist at ambient conditions. For germanium, a similar transition pathway was observed in very specific conditions: during very fast unloading (time<s) in quasi hydrostatic conditions [8]. In this case, the transition to the r8 phase occurs at ~7 GPa and to bc8 at less than 1 GPa.

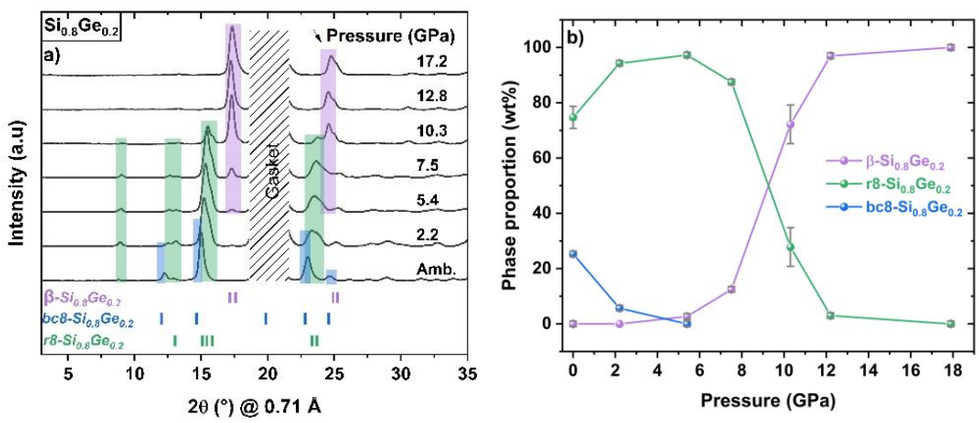

Figure 5 –a) XRD patterns during decompression from 17.2 GPa to ambient pressure of the β-$Si_{0.8}Ge_{0.2}$ phase. Major reflections for each phase are marked in colour. b) Evolution of the phase proportions of the different phases as a function of pressure.

A bulk modulus of K = 80(2) GPa for r8-$Si_{0.8}Ge_{0.2}$ is obtained using a BM2 EOS, in good agreement with the value obtained by *ab initio* simulation (Figure 6). This value is between that of Si (K=83.0(6) GPa) and that of Ge (K = 68.7(3) GPa). It is worth noticing that our

values are lower than those of ref. [11] reporting K = 96(5) with K' = 5 (fixed). Using the K'=5 we obtain K = 76(2) GPa for our experimental results.

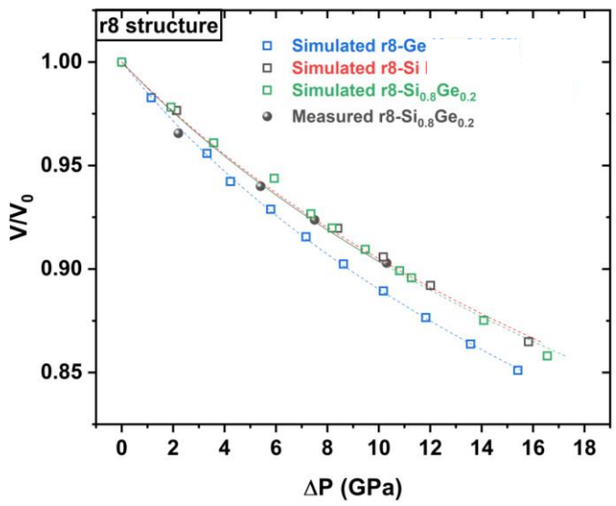

Figure 6 - V/V_0 of r8-$Si_{0.8}Ge_{0.2}$ structure as a function of pressure obtained from this experimental work (black points) along with theoretical data obtained for r8-Si, r8-Ge and r8-$Si_{0.8}Ge_{0.2}$ (open symbols).

The recovered sample is a mixture of bc8 and r8 phases in an almost 75:25 ratio (Figure 7). No trace of other phases could be observed. Such coexistence of r8 and bc8 at ambient pressure has been observed in pure silicon after nano-indentation [76], [77] and in a DAC experiment [72]. The unit cell parameters for r8- and bc8-$Si_{0.8}Ge_{0.2}$ phases at ambient pressure are presented in Table S2. All parameters agree with theoretical values except the *c*-parameter of r8 phase that slightly deviates from expected values (measured at 5.59(1) Å vs 5.649 Å).

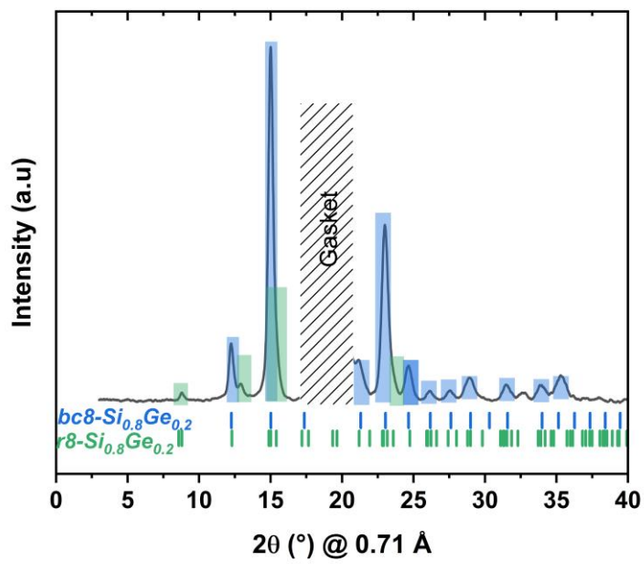

Figure 7 – XRD pattern at ambient conditions of the recovered $Si_{0.8}Ge_{0.2}$ sample after the pressure cycle. LeBail refinement indicates that the sample is composed of two phases: bc8:r8 in a ~75:25 ratio.

To confirm the experimentally observed phase sequence, DFT calculations of enthalpy for the different phases of $Si_{0.8}Ge_{0.2}$ were conducted. Enthalpy variations as a function of pressure for β, bc8 and r8 phases, with the diamond phase as reference, are shown in Figure 8. Enthalpies of the diamond and β phases are predicted to cross at ~9.4 GPa, in good agreement with our experimental data. The kinetics of the phase transition is influenced by temperature and the effect of non-hydrostatic conditions, two parameters that are not included in our simulations. For example, even though the diamond phase is predicted to be the lowest enthalpy structure, r8 phase can be formed during decompression because of a lower kinetic barrier (as shown in the case of Si [78]). In the whole pressure range, the r8 phase has a lower enthalpy than the bc8. Predicted pressure of transition from β to r8 is around 10 GPa in perfect agreement with our experimental results. As pressure is further reduced, enthalpy difference between r8 and bc8 structures decreases by two orders of magnitude, and is almost zero at ambient conditions. This explains the coexistence of the two phases at ambient conditions.

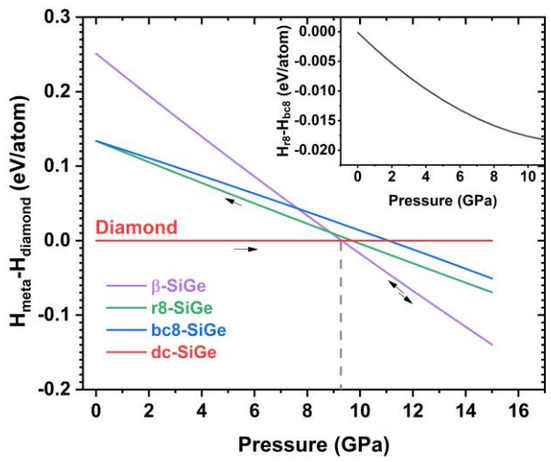

Figure 8 – Enthalpy variations as a function of pressure simulated for different phases of $Si_{0.8}Ge_{0.2}$ The diamond to β structure crossing point is located at 9.3 GPa. The inset represents the enthalpy difference between r8 and bc8 phases, showing that at low pressures the enthalpy difference between the two phases decrease, which could explain the experimentally observed coexistence of r8 and bc8 metastable phase.

C. *In situ* high-pressure Raman spectroscopy

Assignment of the Raman spectrum at ambient conditions

The Raman spectrum of $Si_{0.8}Ge_{0.2}$ measured at ambient conditions is shown in Figure 9. The overall spectrum is in agreement with those from the literature [79]. First, three main peaks are present at ~288, ~405 and ~508 cm^{-1} and correspond to optical phonons associated with Ge-Ge, Ge-Si, and Si-Si vibrations, respectively. These three main modes are asymmetric because of the disorder introduced by the alloying that leads to a partial lifting of the selection rule and a contribution from the vibrational density of states [79], [80]. Using a split Lorentzian function to refine the ratio between left and right full width at half maximum, ratio of 1.58 for Si-Si, 1.86 for Ge-Si and 1.50 for Ge-Ge mode were measured, respectively. Composition determination from peak positions were reported [37], [38]. The most compositionally sensitive peak is the Si-Si. In our sample, it is

measured at 508 cm^{-1} which corresponds to x = 0.19(3) using the method developed in Ref. [38]. This value is in perfect agreement with EDX and XRD results (see section II).

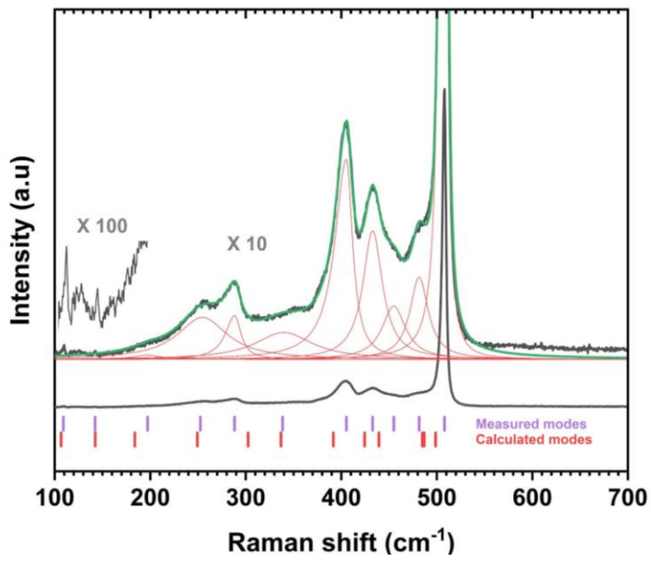

Figure 9 – Typical raw (in black) and fitted (in green) Raman spectrum of diamond-$Si_{0.8}Ge_{0.2}$ at ambient conditions. Low frequencies zone has been magnified x100. Deconvoluted Raman modes are displayed in red. The experimental Raman mode positions (purple ticks) are compared to the Raman frequencies obtained by DFT simulations (red ticks) of a $Si_{0.75}Ge_{0.25}$ alloy.

Between the Ge-Si peak (~405 cm^{-1}) and the Si-Si peak (~508 cm^{-1}), three peaks measured at ~433 cm^{-1}, ~455 cm^{-1} and ~481 cm^{-1} were assigned in the literature to peculiar Si–Si local vibrational modes due to fluctuations of the number of Ge atoms in the vicinity of those of Si [37], [79]. Another peak at ~375 cm^{-1} is not much discussed in the literature and may arise from a local vibration of an isolated Si atom in a Ge matrix [81]. In the low frequency region, a broad feature is observed at ~254 cm^{-1}. This feature is often referred to as quasi-amorphous (q-a) because of a correspondence with a similar peak reported in amorphous alloys [82]. This mode attribution is still under debate [38], [79], [82]. Finally, three very weak peaks in the low frequency region (~197 cm^{-1}, ~142 cm^{-1} and ~109 cm^{-1}) are measured and have not been reported in the literature so far.

All these peaks can be explained in a consistent approach based on DFT simulations as detailed in section II. To complete the study of the vibrational properties, the phonons at the centre of the Brillouin zone were calculated and the symmetry analysis of the eigenvectors for each mode was made in order to identify its possible Raman (R) or infrared (IR) activity. For the ideal diamond structure, the mechanical representation (M) of the normal modes at the center of the Brillouin zone is given by $M = T_{2g}$ (R) + T_{1u} (IR) with the threefold degenerated T_{2g} mode being Raman active. In silicon, this Raman mode is observed at 521 cm^{-1}. However, due to the substitutional disorder, the symmetry is partially lost in the alloys, with the appearance of additional modes and a spurious mode assignment. The analysis of the disordered alloys for each phase within the framework of the band unfolding method can shed light on the real local symmetry of the system and the representation of the irreducible modes (see Section II).

Figure 10 shows the decomposition of the partial spectral function at the center of the Brillouin zone of the disordered Si-Ge alloys for each irreducible representation of the space group (diamond structure) that can be Raman active.

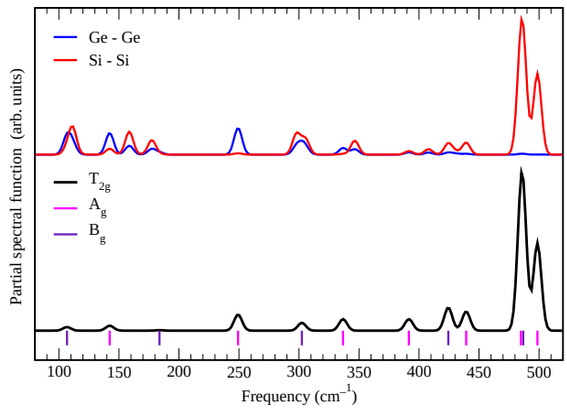

Figure 10 - Decomposition of the partial spectral function at Γ point of the Brillouin zone of disordered $Si_{0.75}Ge_{0.25}$ alloy in the diamond structure. The segments below indicate the positions of the modes obtained from the real disordered structure. In the upper plots the Ge-Ge and Si-Si pairs are represented by blue and red lines, respectively.

The positions of the maxima in the spectral function (Figure 10) are compared with the experimental peak positions in Figure 9. The correspondence between the Raman peaks and the maxima of the simulated partial spectral function is a validation of the method that allows an assignment of all the peaks observed experimentally. By decomposing the spectral function into the contributions of each chemical element, we can deduce the contributions of the Ge and Si to the vibrations of the modes. All peaks above 400 cm^{-1} are mainly related to Si-Si bonds while the peak at 250 cm^{-1} is mainly assigned to Ge-Ge bonds.

Further evidence that this methodology allows to correctly interpret Raman spectra is given by the agreement between simulations and experiments on $Si_{0.8}Ge_{0.2}$ under pressure as developed in the following.

Evolution of Raman spectra upon compression

To complement XRD investigations, HP Raman spectroscopy experiments were conducted on the same alloy. If previous Raman studies have reported the evolution of major Si-Si, Ge-Si or Ge-Ge modes during compression [83], to the best of our knowledge, there is no data on: i) the weak peaks observed in the Raman spectra of the diamond phase (Figure 9); ii) the decompression path; and iii) the vibrational properties of metastable phases obtained upon decompression.

Raman spectra of $Si_{0.8}Ge_{0.2}$ up to 15.7 GPa are reported in Figure 11a). DFT simulations have also been performed over a range of volumes, allowing the theoretical study of the pressure evolution of the frequencies of the different modes. It has to be noticed that during compression, the evolution of the low-frequency modes at ~197, ~142 and ~109 cm^{-1}, observed at ambient pressure, could not be followed due to a weak signal.

Peak positions of the Raman modes of the diamond phase as a function of pressure are reported in Figure 11b and compared to those obtained by *ab initio* simulations. The

positions were fitted using a quadratic equation. The parameters for each mode are given in Table S3.

First, the pressure-induced shifts of the three main modes (Si-Si, Si-Ge, Ge-Ge) are in good agreement with measurements made by Sui *et al.* for similar compositions [83]. Second, the experimental pressure-dependencies are in good agreement with the DFT simulations as shown in Figure 11 (see also Table S3).

In Figure 11a, one can notice that at pressures above ~14 GPa, only a very weak signal from the diamond phase can be measured. The diamond phase transforms to the metallic phase as attested by the electrical resistance measurements (Figure 2c). The Raman cross section of the metallic phase being very low, the signal loss at 15.7 GPa, in our experimental conditions, is a mark of the total disappearance of the diamond phase.

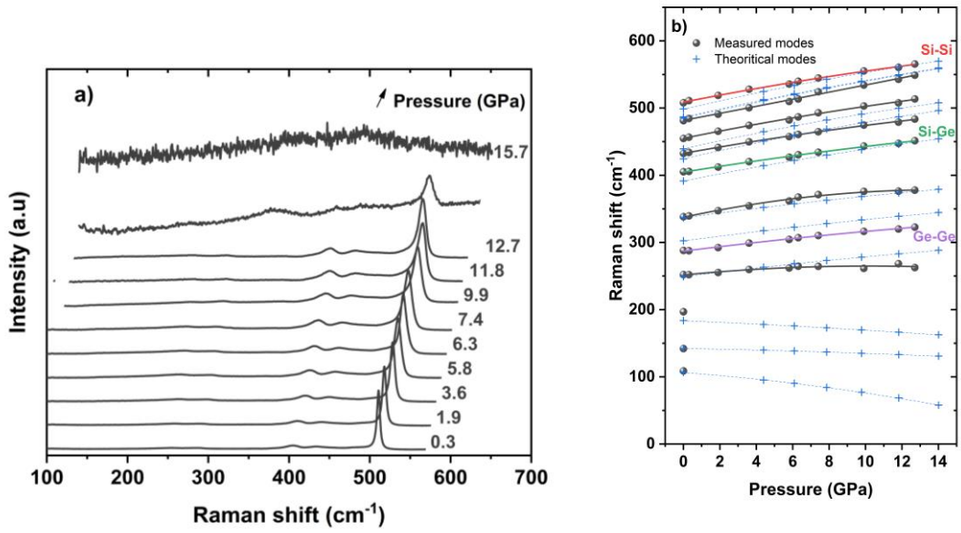

Figure 11 - a) Raman spectra of $Si_{0.8}Ge_{0.2}$ upon compression up to 15.7 GPa showing the transition toward a metallic phase around 15.7 GPa. b) Evolution with increasing pressure of measured $Si_{0.8}Ge_{0.2}$ Raman mode positions along with simulated $Si_{0.75}Ge_{0.25}$ modes projected on an ideal cubic diamond structure. The main Si-Si, Si-Ge and Ge-Ge modes are highlighted in colour.

Evolution of Raman spectra upon decompression

Spectra obtained upon decompression are presented in Figure 12. During decompression, special attention was paid to reducing the laser power to 0.2 mW at the entrance of the objective to minimize sample heating. The exposure time was therefore increased to several hours. During decompression, no significant signal is measured down to ~9.2 GPa, a pressure at which a new spectrum appears. This transition pressure agrees with the β → r8 transition observed by XRD at 10.2 GPa (Figure 5). This spectrum is complex and made of several broad peaks. The main features are: a broad band made of at least two peaks and centered at 310 cm^{-1} and a second band composed of 2-3 peaks and centered at 400 cm^{-1}. Additional peaks at 150 cm^{-1}, 450 cm^{-1} and 550 cm^{-1} are observed. Except for pressure-induced Raman shifts, this new spectrum remains unchanged down to ~3.2 GPa. The pressure-dependencies of the Raman peaks are shown in Figure 12b.

At 0.2 GPa, the spectrum shows new features in addition to reminiscent peaks due to the r8 phase. These new features can be attributed to the bc8-Si phase with peaks at 350 cm^{-1}, bands in the range [400-460 cm^{-1}] and the absence of peaks above 480 cm^{-1}. These features are consistent with those of the bc8-Si [74]. This result indicates that the alloy $Si_{0.8}Ge_{0.2}$ follows a similar transition path to Si, even in the metastable regime.

The partial spectral functions for r8- and bc8-$Si_{0.8}Ge_{0.2}$ at ambient pressure has been simulated (Figure S5). The number of the simulated modes is important. Some of the maxima of the curve coincide with the measured frequencies. The direct assignment is difficult because of the phase coexistence and because the relation between the partial spectral function and the Raman spectra requires consideration of the light-vibration coupling coefficient C(ω), which has an effect on the scattering light. This explains the discrepancies sometimes observed between intensities of simulated modes and experimental data obtained by light scattering [84].

In summary, the sequence of phase transformations under decompression is similar to what observed by XRD, i.e., the phase transition sequence β → r8 → r8+bc8. The absence of strong (Si-Si) mode at 508 cm^{-1} indicates that no diamond phase is present during decompression.

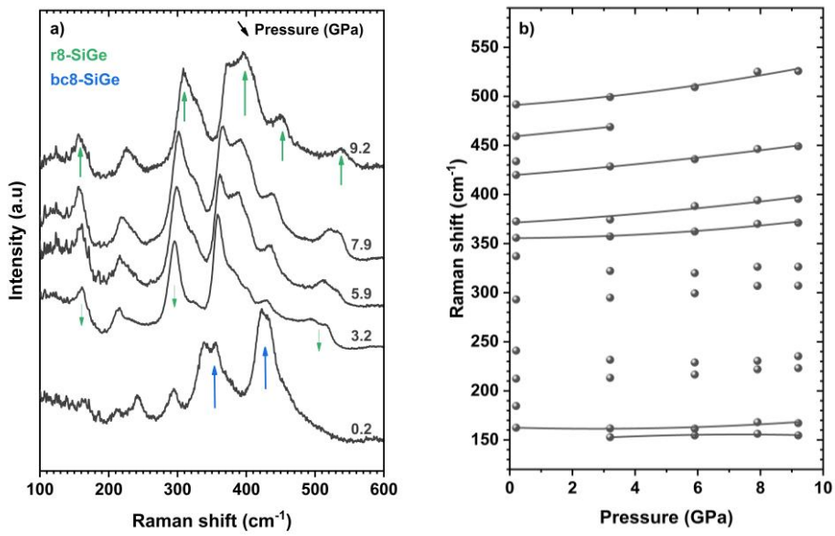

Figure. 12 - (a) Raman spectra of $Si_{0.8}Ge_{0.2}$ sample as a function of pressure during decompression. From 15.7 GPa to ~9.2 GPa, no significant signal is measured and therefore not reported. A new Raman spectrum starts to appear at 9.2 GPa. Green and blue arrows indicate the appearance of the main r8 and bc8 peaks, respectively. (b) Raman frequencies observed in decompression as a function of pressure.

Conclusion

$Si_{0.8}Ge_{0.2}$ alloy has been studied during a pressure cycle. At ambient pressure, the global cubic symmetry is preserved but substitutional disorder strongly modifies the Raman spectra with several additional observed peaks. They can be interpreted using DFT simulations and the band-unfolding method. The experimental pressure-dependencies of the Raman modes are also well reproduced.

By in situ HP XRD experiments we found that the bulk modulus of the $Si_{0.8}Ge_{0.2}$ diamond phase linearly scales with the composition. A pressure-induced phase transition towards

a metallic phase with the β-tin structure is observed with an extended phase coexistence range centered around 12 GPa. The transition towards the β-tin structure can be triggered by isobaric heat treatment.

On decompression, a transition pathway β→r8→r8+bc8 is observed. These metastable phases and this phase transition sequence are similar to those observed in pure silicon. The relative stability of these phases is consistent with DFT simulations. The structural and elastic properties of the r8-phase are also a weighted average between those of Si and Ge.

In conclusion, this work provides an extensive characterization of the $Si_{0.8}Ge_{0.2}$ alloy during pressure cycle. The metastable regime has been accurately investigated for the first time by complementary in situ techniques. The complex Raman spectrum can be now interpreted in a unified manner. Importantly, we provide insights into how to ensure a complete transition to the metallic phase in a large volume press using moderate temperatures, opening up pathway for synthesizing large quantity of metastable phases. This could lead to easier characterisations of the recovered sample using ex-situ characterization techniques and potentially to the scaling up of the metastable phase for various applications.

Acknowledgment

LN2 is a joint International Research Laboratory (IRL 3463) funded and co-operated in Canada by Université de Sherbrooke (UdeS) and in France by CNRS as well as ECL, INSA Lyon, and Université Grenoble Alpes (UGA). It is also supported by the Fonds de Recherche du Québec Nature et Technologie (FRQNT).

The synchrotron X-ray diffraction experiments were performed at the Xpress beamline of Elettra Sincrotrone, Trieste (proposal number: 20210068).

SR acknowledges the support from Spanish MICINN Project No. PID2019-106383GB-43 and the technical expertise and assistance provided by the Spanish Supercomputing Network (Red Española de Supercomputación), as well as the computer resources used: the LaPalma Supercomputer, located at the Instituto de Astrofísica de Canarias.

IV- References

[1] C. S. Menoni, J. Z. Hu, and I. L. Spain, “Germanium at high pressures,” *Phys. Rev. B*, vol. 34, no. 1, pp. 362–368, Jul. 1986, doi: 10.1103/PhysRevB.34.362.

[2] V. V. Brazhkin, A. G. Lyapin, S. V. Popova, and R. N. Voloshin, “Nonequilibrium phase transitions and amorphization in Si, Si/GaAs, Ge, and Ge/GaSb at the decompression of high-pressure phases,” *Phys. Rev. B*, vol. 51, no. 12, pp. 7549–7554, Mar. 1995, doi: 10.1103/PhysRevB.51.7549.

[3] H. Olijnyk, S. K. Sikka, and W. B. Holzapfel, “Structural phase transitions in Si and Ge under pressures up to 50 GPa,” *Phys. Lett. A*, vol. 103, no. 3, pp. 137–140, Jun. 1984, doi: 10.1016/0375-9601(84)90219-6.

[4] X. Yan, D. Tan, X. Ren, W. Yang, D. He, and H.-K. Mao, “Anomalous compression behavior of germanium during phase transformation,” *Appl. Phys. Lett.*, vol. 106, no. 17, p. 171902, Apr. 2015, doi: 10.1063/1.4919003.

[5] G. A. Voronin, C. Pantea, T. W. Zerda, L. Wang, and Y. Zhao, “*In situ* x-ray diffraction study of silicon at pressures up to 15.5 GPa and temperatures up to 1073 K,” *Phys. Rev. B*, vol. 68, no. 2, Jul. 2003, doi: 10.1103/PhysRevB.68.020102.

[6] S. Anzellini, M. T. Wharmby, F. Miozzi, A. Kleppe, D. Daisenberger, and H. Wilhelm, “Quasi-hydrostatic equation of state of silicon up to 1 megabar at ambient temperature,” *Sci. Rep.*, vol. 9, no. 1, Dec. 2019, doi: 10.1038/s41598-019-51931-1.

[7] R. J. Nelmes, M. I. McMahon, N. G. Wright, D. R. Allan, and J. S. Loveday, “Stability and crystal structure of BC8 germanium,” *Phys. Rev. B*, vol. 48, no. 13, pp. 9883–9886, Oct. 1993, doi: 10.1103/PhysRevB.48.9883.

[8] B. Haberl *et al.*, “Controlled formation of metastable germanium polymorphs,” *Phys. Rev. B*, vol. 89, no. 14, Apr. 2014, doi: 10.1103/PhysRevB.89.144111.

[9] J. Z. Hu, L. D. Merkle, C. S. Menoni, and I. L. Spain, “Crystal data for high-pressure phases of silicon,” *Phys. Rev. B*, vol. 34, no. 7, pp. 4679–4684, Oct. 1986, doi: 10.1103/PhysRevB.34.4679.

[10] R. H. Wentorf and J. S. Kasper, “Two New Forms of Silicon,” *Science*, vol. 139, no. 3552, pp. 338–339, 1963, doi: 10.1126/science.139.3552.338.b.

[11] R. O. Piltz, J. R. Maclean, S. J. Clark, G. J. Ackland, P. D. Hatton, and J. Crain, “Structure and properties of silicon XII: A complex tetrahedrally bonded phase,” *Phys. Rev. B*, vol. 52, no. 6, pp. 4072–4085, Aug. 1995, doi: 10.1103/PhysRevB.52.4072.

[12] A. Boucherif, S. Radescu, R. Arès, A. Mujica, P. Mélinon, and D. Machon, “Metastable States in Pressurized Bulk and Mesoporous Germanium,” *J. Phys. Chem. C*, vol. 122, no. 20, pp. 10929–10938, May 2018, doi: 10.1021/acs.jpcc.8b02658.

[13] S. B. Qadri, E. F. Skelton, and A. W. Webb, “High pressure studies of Ge using synchrotron radiation,” *J. Appl. Phys.*, vol. 54, no. 6, pp. 3609–3611, Jun. 1983, doi: 10.1063/1.332434.

[14] E. López-Cruz and M. Cardona, “Raman spectra of two new modifications of germanium: Allo-germanium and 4H-Ge,” *Solid State Commun.*, vol. 45, no. 9, pp. 787–789, 1983, doi: 10.1016/0038-1098(83)90800-1.

[15] L. Q. Huston, B. C. Johnson, B. Haberl, S. Wong, J. S. Williams, and J. E. Bradby, “Thermal stability of simple tetragonal and hexagonal diamond germanium,” *J. Appl. Phys.*, vol. 122, no. 17, p. 175108, Nov. 2017, doi: 10.1063/1.5002705.

[16] R. Braunstein, A. R. Moore, and F. Herman, “Intrinsic Optical Absorption in Germanium-Silicon Alloys,” *Phys. Rev.*, vol. 109, no. 3, pp. 695–710, Feb. 1958, doi: 10.1103/PhysRev.109.695.

[17] J. P. Dismukes, L. Ekstrom, E. F. Steigmeier, I. Kudman, and D. S. Beers, “Thermal and Electrical Properties of Heavily Doped Ge-Si Alloys up to 1300°K,” *J. Appl. Phys.*, vol. 35, no. 10, pp. 2899–2907, Oct. 1964, doi: 10.1063/1.1713126.

[18] C. M. Bhandari and D. M. Rowe, “Silicon–germanium alloys as high-temperature thermoelectric materials,” *Contemp. Phys.*, vol. 21, no. 3, pp. 219–242, May 1980, doi: 10.1080/00107518008210957.

[19] G. Joshi *et al.*, “Enhanced Thermoelectric Figure-of-Merit in Nanostructured p-type Silicon Germanium Bulk Alloys,” *Nano Lett.*, vol. 8, no. 12, pp. 4670–4674, Dec. 2008, doi: 10.1021/nl8026795.

[20] R. L. and G. L., “U.S. Space Radioisotope Power Systems and Applications: Past, Present and Future,” in *Radioisotopes - Applications in Physical Sciences*, N. Singh, Ed., InTech, 2011. doi: 10.5772/23914.

[21] Z. Yu *et al.*, “Improved power conversion efficiency in radial junction thin film solar cells based on amorphous silicon germanium alloys,” *J. Alloys Compd.*, vol. 803, pp. 260–264, Sep. 2019, doi: 10.1016/j.jallcom.2019.06.276.

[22] T. Wood *et al.*, “All-Dielectric Color Filters Using SiGe-Based Mie Resonator Arrays,” *ACS Photonics*, vol. 4, no. 4, pp. 873–883, Apr. 2017, doi: 10.1021/acsphotonics.6b00944.

[23] S. Takagi, “Silicon–germanium (SiGe)-based field effect transistors (FET) and complementary metal oxide semiconductor (CMOS) technologies,” in *Silicon–Germanium (SiGe) Nanostructures*, Elsevier, 2011, pp. 499–527. doi: 10.1533/9780857091420.4.499.
[24] K. Stokes, H. Geaney, G. Flynn, M. Sheehan, T. Kennedy, and K. M. Ryan, “Direct Synthesis of Alloyed $Si_{1-x}Ge_x$ Nanowires for Performance-Tunable Lithium Ion Battery Anodes,” *ACS Nano*, vol. 11, no. 10, pp. 10088–10096, Oct. 2017, doi: 10.1021/acsnano.7b04523.
[25] D. Duveau, B. Fraisse, F. Cunin, and L. Monconduit, “Synergistic Effects of Ge and Si on the Performances and Mechanism of the Ge_xSi_{1-x} Electrodes for Li Ion Batteries,” *Chem. Mater.*, vol. 27, no. 9, pp. 3226–3233, May 2015, doi: 10.1021/cm504413g.
[26] E. M. T. Fadaly *et al.*, “Direct-bandgap emission from hexagonal Ge and SiGe alloys,” *Nature*, vol. 580, no. 7802, pp. 205–209, Apr. 2020, doi: 10.1038/s41586-020-2150-y.
[27] G. Weill, J. L. Mansot, G. Sagon, C. Carlone, and J. M. Besson, “Characterisation of Si III and Si IV, metastable forms of silicon at ambient pressure,” *Semicond. Sci. Technol.*, vol. 4, no. 4, pp. 280–282, Apr. 1989, doi: 10.1088/0268-1242/4/4/029.
[28] J. M. Besson, E. H. Mokhtari, J. Gonzalez, and G. Weill, “Electrical properties of semimetallic silicon III and semiconductive silicon IV at ambient pressure,” *Phys. Rev. Lett.*, vol. 59, no. 4, pp. 473–476, Jul. 1987, doi: 10.1103/PhysRevLett.59.473.
[29] G. Serghiou *et al.*, “Hexagonal Si−Ge Class of Semiconducting Alloys Prepared by Using Pressure and Temperature,” *Chem. – Eur. J.*, vol. 27, no. 57, pp. 14217–14224, Oct. 2021, doi: 10.1002/chem.202102595.
[30] T. Soma, H. Iwanami, and H. Matsuo, “Phase transition under pressure of Si-Ge solid solutions,” *Solid State Commun.*, vol. 42, no. 6, pp. 469–471, May 1982, doi: 10.1016/0038-1098(82)90975-9.
[31] A. Hao, L. Zhang, Z. Gao, Y. Zhu, and L. Riping, “First-principles study of structural stability and elastic properties of the ordered Si0.5Ge0.5 alloy under high pressure,” *Phys. Status Solidi B*, vol. 248, no. 5, pp. 1135–1138, May 2011, doi: 10.1002/pssb.201000745.
[32] G. Queisser and W. B. Holzapfel, “Equation of state data for silicon-germanium alloys under pressures up to 42 GPa,” *Appl. Phys. Solids Surf.*, vol. 53, no. 2, pp. 114–117, Aug. 1991, doi: 10.1007/BF00323869.
[33] G. Queisser, W. A. Grosshans, and W. B. Holzapfel, “Phase Transitions in Silicon-Germanium Alloys under Pressure,” *Europhys. Lett. EPL*, vol. 3, no. 10, pp. 1109–1112, May 1987, doi: 10.1209/0295-5075/3/10/009.
[34] N. V. Morozova, I. V. Korobeinikov, N. V. Abrosimov, and S. V. Ovsyannikov, “Controlling the thermoelectric power of silicon–germanium alloys in different crystalline phases by applying high pressure,” *CrystEngComm*, vol. 22, no. 33, pp. 5416–5435, 2020, doi: 10.1039/D0CE00672F.
[35] Y. Ikeda, A. Carreras, A. Seko, A. Togo, and I. Tanaka, “Mode decomposition based on crystallographic symmetry in the band-unfolding method,” *Phys. Rev. B*, vol. 95, no. 2, Jan. 2017, doi: 10.1103/PhysRevB.95.024305.
[36] F. Körmann, Y. Ikeda, B. Grabowski, and M. H. F. Sluiter, “Phonon broadening in high entropy alloys,” *Npj Comput. Mater.*, vol. 3, no. 1, p. 36, Dec. 2017, doi: 10.1038/s41524-017-0037-8.
[37] D. Rouchon, M. Mermoux, F. Bertin, and J. M. Hartmann, “Germanium content and strain in Si1−xGex alloys characterized by Raman spectroscopy,” *J. Cryst. Growth*, vol. 392, pp. 66–73, Apr. 2014, doi: 10.1016/j.jcrysgro.2014.01.019.
[38] M. I. Alonso and K. Winer, “Raman spectra of *c* - Si 1 − x Ge x alloys,” *Phys. Rev. B*, vol. 39, no. 14, pp. 10056–10062, May 1989, doi: 10.1103/PhysRevB.39.10056.
[39] J. P. Dismukes, L. Ekstrom, and R. J. Paff, “Lattice Parameter and Density in Germanium-Silicon Alloys [1],” *J. Phys. Chem.*, vol. 68, no. 10, pp. 3021–3027, Oct. 1964, doi: 10.1021/j100792a049.
[40] G. Morard *et al.*, “Optimization of Paris-Edinburgh press cell assemblies for in situ monochromatic X-ray diffraction and X-ray absorption,” *HIGH Press. Res.*, vol. 27, no. 2, pp. 223–233, 2007, doi: 10.1080/08957950601183553.
[41] M. Gauthier *et al.*, “High-pressure ultrasonic setup using the Paris–Edinburgh press: Elastic properties of single crystalline germanium up to 6 GPa,” *Rev. Sci. Instrum.*, vol. 74, no. 8, pp. 3712–3716, 2003, doi: 10.1063/1.1593791.
[42] A. D. Chijioke, W. J. Nellis, A. Soldatov, and I. F. Silvera, “The ruby pressure standard to 150GPa,” *J. Appl. Phys.*, vol. 98, no. 11, p. 114905, Dec. 2005, doi: 10.1063/1.2135877.
[43] R. Letoullec, J. P. Pinceaux, and P. Loubeyre, “The membrane diamond anvil cell: A new device for generating continuous pressure and temperature variations,” *High Press. Res.*, vol. 1, no. 1, pp. 77–90, Oct. 1988, doi: 10.1080/08957958808202482.

[44] J. W. Otto, J. K. Vassiliou, and G. Frommeyer, “Nonhydrostatic compression of elastically anisotropic polycrystals. I. Hydrostatic limits of 4:1 methanol-ethanol and paraffin oil,” *Phys. Rev. B*, vol. 57, no. 6, pp. 3253–3263, Feb. 1998, doi: 10.1103/PhysRevB.57.3253.
[45] L. Vegard, “Die Konstitution der Mischkristalle und die Raumfüllung der Atome,” *Z. Phys.*, vol. 5, no. 1, pp. 17–26, Jan. 1921, doi: 10.1007/BF01349680.
[46] L. Vegard, “XV. Die Röntgenstrahlen im Dienste der Erforschung der Materie,” *Z. Für Krist. - Cryst. Mater.*, vol. 67, no. 1–6, pp. 239–259, 1928, doi: doi:10.1524/zkri.1928.67.1.239.
[47] A. R. Denton and N. W. Ashcroft, “Vegard’s law,” *Phys Rev A*, vol. 43, no. 6, pp. 3161–3164, Mar. 1991, doi: 10.1103/PhysRevA.43.3161.
[48] A. van de Walle, M. Asta, and G. Ceder, “The alloy theoretic automated toolkit: A user guide,” *Calphad*, vol. 26, no. 4, pp. 539–553, 2002, doi: 10.1016/S0364-5916(02)80006-2.
[49] A. van de Walle, “Multicomponent multisublattice alloys, nonconfigurational entropy and other additions to the Alloy Theoretic Automated Toolkit,” *Calphad*, vol. 33, no. 2, pp. 266–278, Jun. 2009, doi: 10.1016/j.calphad.2008.12.005.
[50] J. P. Perdew *et al.*, “Restoring the Density-Gradient Expansion for Exchange in Solids and Surfaces,” *Phys Rev Lett*, vol. 100, no. 13, p. 136406, Apr. 2008, doi: 10.1103/PhysRevLett.100.136406.
[51] G. Kresse and J. Hafner, “*Ab initio* molecular dynamics for liquid metals,” *Phys. Rev. B*, vol. 47, no. 1, pp. 558–561, Jan. 1993, doi: 10.1103/PhysRevB.47.558.
[52] G. Kresse and J. Furthmüller, “Efficient iterative schemes for *ab initio* total-energy calculations using a plane-wave basis set,” *Phys. Rev. B*, vol. 54, no. 16, pp. 11169–11186, Oct. 1996, doi: 10.1103/PhysRevB.54.11169.
[53] G. Kresse and J. Furthmüller, “Efficiency of ab-initio total energy calculations for metals and semiconductors using a plane-wave basis set,” *Comput. Mater. Sci.*, vol. 6, no. 1, pp. 15–50, Jul. 1996, doi: 10.1016/0927-0256(96)00008-0.
[54] A. Togo and I. Tanaka, “First principles phonon calculations in materials science,” *Scr. Mater.*, vol. 108, pp. 1–5, Nov. 2015, doi: 10.1016/j.scriptamat.2015.07.021.
[55] K. Momma and F. Izumi, “*VESTA 3* for three-dimensional visualization of crystal, volumetric and morphology data,” *J. Appl. Crystallogr.*, vol. 44, no. 6, pp. 1272–1276, Dec. 2011, doi: 10.1107/S0021889811038970.
[56] S. Minomura and H. G. Drickamer, “Pressure induced phase transitions in silicon, germanium and some III–V compounds,” *J. Phys. Chem. Solids*, vol. 23, no. 5, pp. 451–456, May 1962, doi: 10.1016/0022-3697(62)90085-9.
[57] R. J. Needs and R. M. Martin, “Transition from \ensuremath\beta-tin to simple hexagonal silicon under pressure,” *Phys Rev B*, vol. 30, no. 9, pp. 5390–5392, Nov. 1984, doi: 10.1103/PhysRevB.30.5390.
[58] L. L. Boyer, E. Kaxiras, J. L. Feldman, J. Q. Broughton, and M. J. Mehl, “New low-energy crystal structure for silicon,” *Phys Rev Lett*, vol. 67, no. 6, pp. 715–718, Aug. 1991, doi: 10.1103/PhysRevLett.67.715.
[59] R. J. Needs and A. Mujica, “First-principles pseudopotential study of the structural phases of silicon,” *Phys Rev B*, vol. 51, no. 15, pp. 9652–9660, Apr. 1995, doi: 10.1103/PhysRevB.51.9652.
[60] A. Werner, J. A. Sanjurjo, and M. Cardona, “X-rays investigation of the α→β phase transition in the GexSi1−x solid solutions at high pressure,” *Solid State Commun.*, vol. 44, no. 2, pp. 155–158, 1982, doi: https://doi.org/10.1016/0038-1098(82)90420-3.
[61] G. Ackland, “High-pressure phases of group IV and III-V semiconductors,” *Rep. Prog. Phys.*, vol. 64, pp. 483–516, Apr. 2001, doi: 10.1088/0034-4885/64/4/202.
[62] A. Kubo *et al.*, “Melting curve of silicon to 15GPa determined by two-dimensional angle-dispersive diffraction using a Kawai-type apparatus with X-ray transparent sintered diamond anvils,” *J. Phys. Chem. Solids*, vol. 69, no. 9, pp. 2255–2260, Sep. 2008, doi: 10.1016/j.jpcs.2008.04.025.
[63] M. I. McMahon, R. J. Nelmes, N. G. Wright, and D. R. Allan, “Pressure dependence of the *Imma* phase of silicon,” *Phys. Rev. B*, vol. 50, no. 2, pp. 739–743, Jul. 1994, doi: 10.1103/PhysRevB.50.739.
[64] H. J. McSkimin and P. Andreatch, “Elastic Moduli of Germanium Versus Hydrostatic Pressure at 25.0°C and −195.8°C,” *J. Appl. Phys.*, vol. 34, no. 3, pp. 651–655, Mar. 1963, doi: 10.1063/1.1729323.
[65] M. Senoo, H. Mii, I. Fujishiro, and T. Fujikawa, “Precise Measurements of Lattice Compression of Al, Si and Al-Si Alloys by High Pressure X-Ray Diffractometry,” *Jpn. J. Appl. Phys.*, vol. 15, no. 5, p. 871, May 1976, doi: 10.1143/JJAP.15.871.
[66] W. B. Gauster, “Grüneisen parameters of germanium-silicon alloy,” *J. Appl. Phys.*, vol. 44, no. 3, pp. 1089–1091, Mar. 1973, doi: 10.1063/1.1662310.
[67] D. Machon, F. Meersman, M. C. Wilding, M. Wilson, and P. F. McMillan, “Pressure-induced amorphization and polyamorphism: Inorganic and biochemical systems,”

Prog. Mater. Sci., vol. 61, pp. 216–282, Apr. 2014, doi: 10.1016/j.pmatsci.2013.12.002.
[68] “Silvia Pandolfi. High-pressure pathways towards new functional Si-based materials with tailored optoelectronic properties and their characterization. Materials Science [cond-mat.mtrl-sci]. Sorbonne Université, 2019. English. ⟨NNT : 2019SORUS459⟩. ⟨tel-03480902⟩.”
[69] A. Mujica, A. Rubio, A. Muñoz, and R. J. Needs, “High-pressure phases of group-IV, III–V, and II–VI compounds,” *Rev Mod Phys*, vol. 75, no. 3, pp. 863–912, Jul. 2003, doi: 10.1103/RevModPhys.75.863.
[70] H. Olijnyk, “Raman scattering in metallic Si and Ge up to 50 GPa,” *Phys. Rev. Lett.*, vol. 68, no. 14, pp. 2232–2234, Apr. 1992, doi: 10.1103/PhysRevLett.68.2232.
[71] M. Y. Lv, Z. W. Chen, R. P. Liu, and W. K. Wang, “Ab initio study of pressure-induced phase transitions in the ordered Si50Ge50 alloy,” *Solid State Commun.*, vol. 135, no. 11, pp. 749–752, 2005, doi: https://doi.org/10.1016/j.ssc.2005.05.013.
[72] J. Crain, G. J. Ackland, J. R. Maclean, R. O. Piltz, P. D. Hatton, and G. S. Pawley, “Reversible pressure-induced structural transitions between metastable phases of silicon,” *Phys. Rev. B*, vol. 50, no. 17, pp. 13043–13046, Nov. 1994, doi: 10.1103/PhysRevB.50.13043.
[73] A. Wosylus, H. Rosner, W. Schnelle, and U. Schwarz, “Crystal Structure Refinement and Electronic Properties of Si(cI16),” *Z. Für Anorg. Allg. Chem.*, vol. 635, no. 4–5, pp. 700–703, 2009, doi: https://doi.org/10.1002/zaac.200900051.
[74] O. O. Kurakevych *et al.*, “Synthesis of Bulk BC8 Silicon Allotrope by Direct Transformation and Reduced-Pressure Chemical Pathways,” *Inorg. Chem.*, vol. 55, no. 17, pp. 8943–8950, Sep. 2016, doi: 10.1021/acs.inorgchem.6b01443.
[75] G. Serghiou *et al.*, “Dense SixGe1–x (0 < x < 1) Materials Landscape Using Extreme Conditions and Precession Electron Diffraction,” *Inorg. Chem.*, vol. 53, no. 11, pp. 5656–5662, Jun. 2014, doi: 10.1021/ic500416s.
[76] A. Kailer, Y. G. Gogotsi, and K. G. Nickel, “Phase transformations of silicon caused by contact loading,” *J. Appl. Phys.*, vol. 81, no. 7, pp. 3057–3063, Apr. 1997, doi: 10.1063/1.364340.
[77] D. Ge, V. Domnich, and Y. Gogotsi, “Thermal stability of metastable silicon phases produced by nanoindentation,” *J. Appl. Phys.*, vol. 95, no. 5, pp. 2725–2731, Mar. 2004, doi: 10.1063/1.1642739.
[78] J.-T. Wang, C. Chen, H. Mizuseki, and Y. Kawazoe, “Kinetic Origin of Divergent Decompression Pathways in Silicon and Germanium,” *Phys. Rev. Lett.*, vol. 110, no. 16, p. 165503, Apr. 2013, doi: 10.1103/PhysRevLett.110.165503.
[79] S. Rath, M. L. Hsieh, P. Etchegoin, and R. A. Stradling, “Alloy effects on the Raman spectra of $Si_{1-x}Ge_x$ and calibration protocols for alloy compositions based on polarization measurements,” *Semicond. Sci. Technol.*, vol. 18, no. 6, pp. 566–575, Jun. 2003, doi: 10.1088/0268-1242/18/6/330.
[80] A. S. Barker and A. J. Sievers, “Optical studies of the vibrational properties of disordered solids,” *Rev. Mod. Phys.*, vol. 47, no. S2, pp. S1–S179, Jan. 1975, doi: 10.1103/RevModPhys.47.S1.2.
[81] O. Pagès, R. H. Hussein, and V. J. B. Torres, “GeSi Raman spectra vs. local clustering/anticlustering: Percolation scheme and *ab initio* calculations,” *J. Appl. Phys.*, vol. 114, no. 3, p. 033513, Jul. 2013, doi: 10.1063/1.4813513.
[82] J. S. Lannin, “Chapter 6 Raman Scattering of Amorphous Si, Ge, and Their Alloys,” in *Semiconductors and Semimetals*, Elsevier, 1984, pp. 159–195. doi: 10.1016/S0080-8784(08)62914-2.
[83] Z. Sui, H. H. Burke, and I. P. Herman, “Raman scattering in germanium-silicon alloys under hydrostatic pressure,” *Phys. Rev. B*, vol. 48, no. 4, pp. 2162–2168, Jul. 1993, doi: 10.1103/PhysRevB.48.2162.
[84] R. Shuker and R. W. Gammon, “Raman-Scattering Selection-Rule Breaking and the Density of States in Amorphous Materials,” *Phys Rev Lett*, vol. 25, no. 4, pp. 222–225, Jul. 1970, doi: 10.1103/PhysRevLett.25.222.